AIAA JOURNAL
Vol. 35, No. 8, August 1997

Consistent Methodology for the Modeling of Piezolaminated Shells

Baruch Pletner* and Haim Abramovich†
Technion—Israel Institute of Technology, Haifa 32000, Israel

A consistent methodology is developed and presented for the modeling of the static and dynamic response of anisotropic piezolaminated shells with spatially discrete sensors and actuators. The theory on which the methodology is based is general and can be applied to any piezolaminated shell within the confines of the Kirchhoff–Love thin shell theory. The methodology provides effective tools for replacing the piezoelectric induced-strain loading of the structure with an equivalent mechanical loading. Additionally, it yields the governing equations for the static and dynamic structural response to piezoelectric loading. An indexing technique for structural, actuating, and sensing laminae is proposed. Nondimensional coefficients, which illustrate the actuating capability of the piezoactuators, as well as their relative stiffnesses, are used. The general methodology is applied to laminates with one structural lamina with piezoelectric actuators bonded to one or both of its surfaces. The analytical results are compared with results yielded by the ANSYS® finite element program for a rectangular isotropic plate and a cylindrical panel. The plate case was also investigated experimentally. Excellent agreement is demonstrated between the finite element, experimental, and analytical results.

Introduction

A COMMON form of intelligent or adaptive structures are thin shells equipped with piezoelectric laminae. These laminae are made of piezoelectric materials such as lead zirconate titanate (PZT) and are capable of transducing electric fields into mechanical strains and mechanical strains into electric charges. These active laminae are used to actuate the shell by inducing strains in the nonpiezoelectric passive laminae and to sense deflections in the shell by measuring the local strain fields. The active laminae can be continuous over the entire domain of the structure or discontinuous as in the case of piezoceramic patches. Sufficiently accurate models for induced strain actuation are essential for the design of intelligent structures and their use for vibration suppression and steering.

The importance of these models was recognized in the literature, where they received wide attention. The so-called pin-force models were originated in the pioneering work by Crawley and de Luis,[1] which assessed the contribution of a finite bonding layer to the model's accuracy, neglecting, however, the stiffness contribution of the piezoelectric material. This model was applied to isotropic beams and plates consisting of a single passive lamina, with one or two actuators bonded to its upper and lower surfaces. The pin-force model was further extended by Chaudhry and Rogers[2] and Strambi et al.[3] to include the stiffness of the piezoelectric material in the expressions for the induced strain. Dimitriadis et al.[4] employed the extended pin-force model to obtain the dynamic response of a simply supported isotropic plate to induced strain actuation, and Wang and Rogers[5] extended the model for anisotropic laminated shells with embedded piezoceramic patches. These works were experimentally validated by Clark et al.[6] A comprehensive theory for piezolaminated shells with spatially continuous piezoelectric laminae was developed by Tzou,[7] who also presented the shells' equations of motion.

The possibility of actuating and detecting torsional motion by skewing the dominant rolling axis angle of the piezoelectric elements with respect to the structural axes was investigated by Miller et al.,[8,9] Pletner and Abramovich,[10,11] and Park et al.,[12] among others. The skew angle is an important design parameter, especially for anisotropic media, and should be incorporated into the intelligent structure design process to excite and detect torsional modes, as well as avoid unwanted coupling effects. Current work addresses this by allowing arbitrary skew angles in the general formulation. The particular case of piezoactuated cylindrical shells was addressed by Sonti and Jones[13] and is in agreement with the results derived in the current work from the general theory of actuated shells.

The collected literature on the pin-force model of induced strain actuation as previously presented suffers from lack of generality and can be confusing to structural analysts who are used to finding the response of structures to mechanical excitations. Can induced strain actuators be replaced by forces or moments; should the stiffness and mass contributions of the actuators be included in the structural models; what are the effects of the positioning of the active laminae within the laminated shell? These, among others, are questions that need to be addressed, before structural design incorporating active laminae is to be attempted.

A general theory for the behavior of thin anisotropic laminated shells of arbitrary geometry and boundary conditions under spatially continuous induced strain actuation was developed by Miller et al.[8,9] Their work presented closed-form solutions for actuated shells, which are both materially and geometrically continuous in the in-plane directions. This assumption breaks down when the active laminae consist of geometrically discrete patches, and the stiffness and mass contributions of these patches are too significant to be neglected. In current work this theory is extended to accomodate material and geometric variations, and the resulting equations of motion are presented in a normalized form, which facilitates the decision on the inclusion or exclusion of the mass and stiffness contributions of the actuator patches.

When the shell's geometric or material properties vary in the in-plane directions, as well as for many types of boundary conditions, the equations of motion do not yield to closed-form solutions. For those cases the current work presents the equations of motion in a form readily accessible for solution by well-established approximate methods, as well as yielding the equivalent mechanical loads produced by the piezoelectric actuators for inclusion in a finite element code.

General Model for Actuation and Sensing in Thin Anisotropic Piezolaminated Shells

In this section the static and dynamic response of piezolaminated shells is developed and presented. A piezolaminated shell is defined as a thin anisotropic laminated shell, which possesses one or more

Received July 29, 1996; revision received April 25, 1997; accepted for publication May 6, 1997.

*Graduate Student, Faculty of Aerospace Engineering. Student Member AIAA.

†Senior Lecturer, Faculty of Aerospace Engineering; currently Visiting Professor, Institute for Lightstructures and Ropeways, ETH Zürich, Leonhardstrasse 25 LEC, Zurich CH-8992, Switzerland. Senior Member AIAA.

piezoelectric laminae. We denote these laminae as active laminae when they are used for actuation and as sensory laminae when they are used for sensing. In the case of self-sensing actuation, they will be denoted self-sensing active laminae. The piezoelectric laminae need not span the entire structural plane. As a matter of fact, in reality they will in many cases constitute subareas, or patches, in the total area of the shell. An area of the shell that has one or more active laminae will be called actuated area, and an area which has one or more sensory laminae will be called sensory area. These areas will be numbered with the indices $n = 1, \ldots, N_a$ and $m = 1, \ldots, N_m$, respectively. The structural laminae in the shell will be numbered with the index i, the active laminae with the index j, and the sensory laminae with the index l. The index k will be used to number laminae regardless of their purpose. For example, a particular area of the shell may be both actuated and sensory with a total number of six laminae, out of which $i = 3$ and 4 are structural laminae, $j = 2$ and 5 are active laminae, and $l = 1$ and 6 are sensory laminae. This example is illustrated in Fig. 1a.

The theory presented in this chapter applies to shells in which the following governing assumptions are valid. 1) The strain-displacement relations are linear. 2) The shear deformations in the shell are neglected (the Kirchhoff hypothesis). 3) The ratio of shell thickness to radii of curvature is small ($h_t/R_1, h_t/R_2 \ll 1$). 4) The state of the plane stress is assumed; transverse strains are neglected. 5) Mass and stiffness properties of each lamina do not vary in the thickness direction. 6) Bonding between laminae is perfect and infinitesimally thin.

Stress–Strain Relations

The principle of operation of piezoelectric materials can be written concisely as

$$\begin{Bmatrix} \boldsymbol{T} \\ D \end{Bmatrix} = \begin{bmatrix} c & e \\ e^T & -\varepsilon \end{bmatrix} \begin{Bmatrix} \boldsymbol{S} \\ -E \end{Bmatrix} \tag{1}$$

These principles apply to the active as well as passive laminae within a general laminated shell, as shown in Fig. 1b. For the passive laminae, the piezoelectric constitutive parameters vectors e and ε are formally set to zero, and Eq. (1) is reduced to generalized Hooke's law $\boldsymbol{T} = c\boldsymbol{S}$.

Within the assumptions of the Kirchhoff–Love first approximation shell theory, as just presented, we define a general shell in a curvilinear orthogonal coordinate system defined by the unit vectors $\hat{\boldsymbol{\alpha}}_i$, $i = 1, 2, 3$. Generally, the elastic coefficients matrix of the kth lamina is given in a coordinate system that does not coincide with the coordinate system of the entire structure, and a transformation is required. Assuming that the elastic properties of the kth lamina are quoted in a coordinate system that is rotated by angle θ^k, with respect to the structural coordinate system, the transformed elastic coefficients matrix for this lamina can be obtained from the original matrix c_0^k as

$$c^k = T_1^{-1} c_0^k T_2 \tag{2}$$

where

$$T_1 = \begin{bmatrix} m^2 & n^2 & 2mn \\ n^2 & m^2 & -2mn \\ -mn & mn & m^2 - n^2 \end{bmatrix} \tag{3}$$

$$T_2 = \begin{bmatrix} m^2 & n^2 & mn \\ n^2 & m^2 & -mn \\ -2mn & 2mn & m^2 - n^2 \end{bmatrix} \tag{4}$$

and $n = \sin\theta^k$ and $m = \cos\theta^k$.

The piezoelectric displacement vector of the kth lamina in the structural coordinates is given by

$$\boldsymbol{d}_0^k = \begin{Bmatrix} d_{31} \\ d_{32} \\ 0 \end{Bmatrix}^k \tag{5}$$

and the piezoelectric constitutive parameters vector is defined as

$$\boldsymbol{e}_0^k = \begin{Bmatrix} e_{31} \\ e_{32} \\ e_{36} \end{Bmatrix}^k \triangleq T_1^{-1} c_0^k \boldsymbol{d}_0^k \tag{6}$$

For isotropic and orthotropic materials (for which the principal material and structural axes coincide), the shear term e_{36} vanishes when T_1 is an identity matrix. This means that the piezoelectric element cannot sense or excite shear strains and stresses in the shell. When such excitation or sensing is desirable, the dominant rolling axis of the piezoelectric laminae should be skewed with respect to the structural axes. Alternatively, the piezoelectric element can be bonded to the structural lamina in such a way that its dominant rolling axis does not coincide with the structural axes. Both methods result in a transformation matrix that makes $e_{36} \neq 0$. For general anisotropic materials, in which the normal and shear stresses are coupled through the material properties, $e_{36} \neq 0$ for all values of T_1.

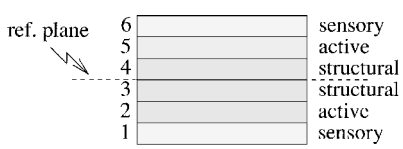

Fig. 1a Possible arrangement of active sensing and structural laminae.

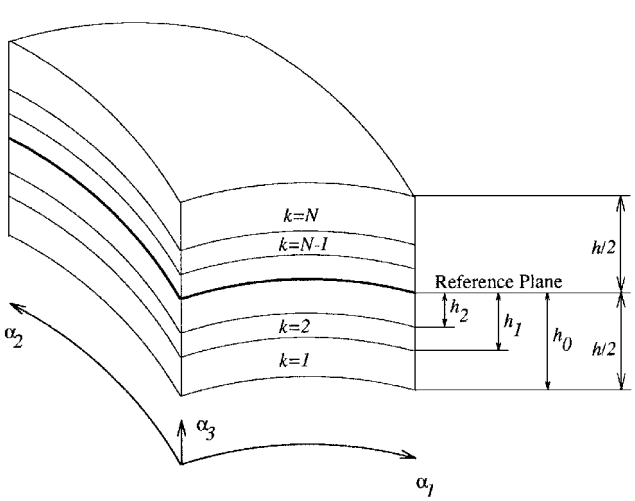

Fig. 1b General laminated shell.

Strain-Displacement Relations

Following accepted notation, we denote as U, V, W the displacements of an arbitrary point in the shell in each of the directions $\hat{\boldsymbol{\alpha}}_i$, $i = 1, 2, 3$, respectively. The angles of rotation are denoted as β_i, $i = 1, 2, 3$. Because the displacements are assumed constant in the thickness direction of the shell, they can be written as

$$\begin{Bmatrix} U(\alpha_1, \alpha_2, \alpha_3) \\ V(\alpha_1, \alpha_2, \alpha_3) \\ W(\alpha_1, \alpha_2, \alpha_3) \end{Bmatrix} = \begin{Bmatrix} u(\alpha_1, \alpha_2) \\ v(\alpha_1, \alpha_2) \\ w(\alpha_1, \alpha_2) \end{Bmatrix} + \alpha_3 \begin{Bmatrix} \beta_1(\alpha_1, \alpha_2) \\ \beta_2(\alpha_1, \alpha_2) \\ 0 \end{Bmatrix} \tag{7}$$

where u, v, w represent the displacements of any given point on the reference plane of the shell. The angles of rotation are given by

$$\begin{Bmatrix} \beta_1 \\ \beta_2 \end{Bmatrix} = \begin{Bmatrix} (1/R_1)u - (1/A_1)w_{,\alpha_1} \\ (1/R_2)v - (1/A_2)w_{,\alpha_2} \end{Bmatrix} \tag{8}$$

and the curvatures are defined as

$$\kappa = \begin{Bmatrix} \dfrac{1}{A_1}\dfrac{\partial \beta_1}{\partial \alpha_1} + \dfrac{\beta_2}{A_1 A_2}\dfrac{\partial A_1}{\partial \alpha_2} \\ \dfrac{1}{A_2}\dfrac{\partial \beta_2}{\partial \alpha_2} + \dfrac{\beta_1}{A_1 A_2}\dfrac{\partial A_2}{\partial \alpha_1} \\ \dfrac{A_2}{A_1}\dfrac{\partial}{\partial \alpha_1}\left(\dfrac{\beta_2}{A_2}\right) + \dfrac{A_1}{A_2}\dfrac{\partial}{\partial \alpha_2}\left(\dfrac{\beta_1}{A_1}\right) \end{Bmatrix} \tag{9}$$

Table 1 Lamé parameters and radii of curvature for common shell geometries

Geometry	A_1	A_2	R_1	R_2
Flat plate	1	1	∞	∞
Circular cylindrical shell	1	a	∞	a
Arch	1	1	$R_1(\alpha_1)$	∞
Circular ring	1	1	a	∞
Shells of revolution	R_1	$R_2 \sin\alpha_1$	$R_1(\alpha_1)$	$R_2(\alpha_2)$

where A_1, A_2, and R_1, R_2 are the Lamé parameters and radii of curvature, respectively. The Lamé parameters and radii of curvature for several commonly found shell geometries are presented in Table 1, where a is the shell radius.

The strain vector of a thin shell consists of the contributions of the stretching of the reference plane ϵ_0, and the curvatures vector κ. This can be written explicitly for the kth lamina as

$$\epsilon_k = [I_3 \mid \alpha_3 I_3]\begin{Bmatrix}\epsilon_0\\ \kappa\end{Bmatrix} = [I_3 \mid \alpha_3 I_3]\left(\frac{1}{A_1 A_2}\mathcal{E}\right) \tag{10}$$

where I_3 is an identity matrix of rank three and $\mathcal{E}$ is a homogeneous linear differential operator defined as

$$\mathcal{E} = [\mathcal{E}^1 \mid \mathcal{E}^2] \tag{11}$$

where

$$\mathcal{E}^1 \triangleq \begin{bmatrix} A_2\frac{\partial}{\partial\alpha_1} & \frac{\partial A_1}{\partial\alpha_2}\\ \frac{\partial A_2}{\partial\alpha_1} & A_1\frac{\partial}{\partial\alpha_2}\\ A_1^2\frac{\partial}{\partial\alpha_2}\cdot\frac{1}{A_1} & A_2^2\frac{\partial}{\partial\alpha_1}\cdot\frac{1}{A_2}\\ A_2^2\frac{\partial}{\partial\alpha_1}\cdot\frac{1}{R_1} & \frac{\partial A_1}{\partial\alpha_2}\frac{1}{R_2}\\ \frac{\partial A_2}{\partial\alpha_1}\frac{1}{R_1} & A_1^2\frac{\partial}{\partial\alpha_2}\cdot\frac{1}{R_2}\\ A_1^2\frac{\partial}{\partial\alpha_2}\cdot\frac{1}{A_1 R_1} & A_2^2\frac{\partial}{\partial\alpha_1}\cdot\frac{1}{A_2 R_2}\end{bmatrix} \tag{12}$$

$$\mathcal{E}^T \triangleq \left[\begin{array}{ccc|ccc}\frac{A_1 A_2}{R_1} & \frac{A_1 A_2}{R_1} & 0 & \mathcal{E}^1 & \mathcal{E}^2 & \mathcal{E}^3\end{array}\right] \tag{13}$$

and

$$\mathcal{E}^1 = -\left(A_2\frac{\partial}{\partial\alpha_1}\cdot\frac{1}{A_1}\cdot\frac{\partial}{\partial\alpha_1} + \frac{1}{A_2}\frac{\partial A_1}{\partial\alpha_2}\frac{\partial}{\partial\alpha_2}\right) \tag{14}$$

$$\mathcal{E}^2 = -\left(A_1\frac{\partial}{\partial\alpha_2}\cdot\frac{1}{A_2}\cdot\frac{\partial}{\partial\alpha_2} + \frac{1}{A_1}\frac{\partial A_2}{\partial\alpha_1}\frac{\partial}{\partial\alpha_1}\right) \tag{15}$$

$$\mathcal{E}^3 = -\left(A_2^2\frac{\partial}{\partial\alpha_1}\cdot\frac{1}{A_2^2}\cdot\frac{\partial}{\partial\alpha_2} + \frac{1}{A_1^2}\frac{\partial A_2}{\partial\alpha_2}\frac{1}{A_1^2}\frac{\partial}{\partial\alpha_1}\right) \tag{16}$$

and $\boldsymbol{x} = [u \mid v \mid w]^T$ is the reference plane displacement vector.

Free Strain Induced-Strain Relations

Because the stress at any given point in the shell is a combination of the mechanical and piezoelectrically induced stresses [Eq. (1)], the normal force resultants and moments in a cross section of the shell can also be expressed as such a combination:

$$\begin{Bmatrix}\boldsymbol{N}\\ \boldsymbol{M}\end{Bmatrix} = \begin{Bmatrix}\boldsymbol{N}\\ \boldsymbol{M}\end{Bmatrix}_s - \begin{Bmatrix}\boldsymbol{N}\\ \boldsymbol{M}\end{Bmatrix}_a \tag{17}$$

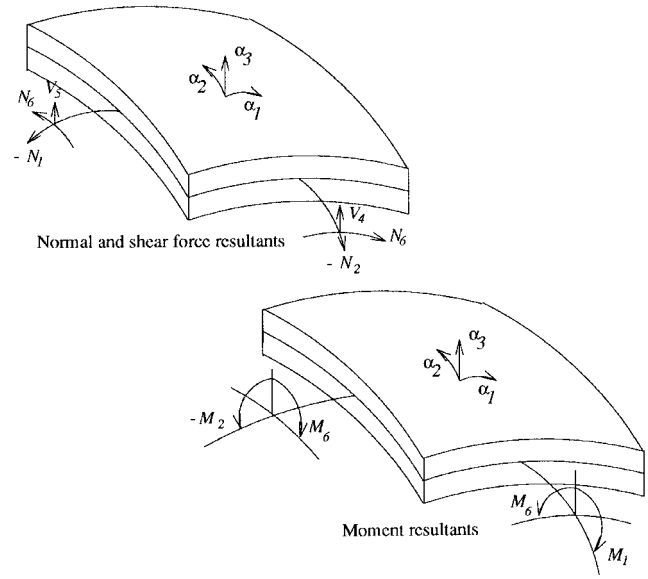

Fig. 2 Definition of in-plane and transverse force and moment resultants.

This leads to the formulation of the resultant forces and moments in the shell as

$$\begin{Bmatrix}\boldsymbol{N}\\ \boldsymbol{M}\end{Bmatrix} = \sum_{k=1}^{N}\int_{h_{k-1}}^{h_k}\begin{bmatrix}c^k & \alpha_3 c^k\\ \alpha_3 c^k & \alpha_3^2 c^k\end{bmatrix}\begin{Bmatrix}\epsilon_0\\ \kappa\end{Bmatrix}\mathrm{d}\alpha_3 - \sum_{k=1}^{N}\int_{h_{k-1}}^{h_k}\begin{Bmatrix}I_3\\ \alpha_3 I_3\end{Bmatrix}\boldsymbol{e}^k E_3^k\,\mathrm{d}\alpha_3 \tag{18}$$

The force and moment resultants in the shell are defined as in Fig. 2.

Keeping in mind that the curvatures do not vary in the thickness direction and that the electromechanical properties of each lamina are also constant in that direction, Eq. (18) can be rewritten in terms of the free strain as

$$\begin{Bmatrix}\boldsymbol{N}(\alpha_1,\alpha_2)\\ \boldsymbol{M}(\alpha_1,\alpha_2)\end{Bmatrix} = C_t\begin{Bmatrix}\epsilon_0\\ \kappa\end{Bmatrix} - L(\alpha_1,\alpha_2) \tag{19}$$

where C_t is a generalized stiffness matrix and $\boldsymbol{L}(\alpha_1,\alpha_2)$ is the total induced-strain loading of the structure. The generalized stiffness matrix consists of the contributions of the laminae to the axial and bending stiffnesses of the shell cross section. The active laminae are often made of discrete patches, which do not span the entire surface of the shell. The contributions of these laminae to the mass and stiffness of the shell are often neglected to facilitate closed-form solutions. Therefore, it is advantageous to represent the total stiffness matrix C_t as a sum of the contributions of the continuous passive laminae C_s and those of the (possibly discrete) active laminae C_a. The resulting matrices assume the form

$$C_t = C_s + C_a\sum^{N_a} S_{\alpha_1}^n(\alpha_1)S_{\alpha_2}^n(\alpha_2) \tag{20}$$

where $S_{\alpha_1}^n(\alpha_1)$ and $S_{\alpha_2}^n(\alpha_2)$ are functions that describe the spatial distribution of the nth actuated area in the shell, which are given subsequently. The stiffness matrices are given by

$$C_{s,a} = \left[\begin{array}{c|c}A_{s,a} & B_{s,a}\\ \hline B_{s,a} & D_{s,a}\end{array}\right] \tag{21}$$

where

$$A_{s,a} = (h_{i,j} - h_{i,j-1})c^{i,j} \tag{22}$$

$$B_{s,a} = \tfrac{1}{2}(h_{i,j}^2 - h_{i,j-1}^2)\,c^{i,j} \tag{23}$$

$$D_{s,a} = \tfrac{1}{3}(h_{i,j}^3 - h_{i,j-1}^3)\,c^{i,j} \tag{24}$$

where the index i relates to the passive laminae and the index j to the active laminae. The diagonal blocks A and D constitute the axial and

bending stiffnesses of the shell, respectively, and the off-diagonal blocks B the coupled stiffnesses. In case of structures in which the bending and axial stresses are uncoupled, C is block diagonal. As will be shown later, this is the case with laminates that are arranged symmetrically about the reference plane.

The generalized induced strain load vector produced by the nth actuated area $L_n(\alpha_1, \alpha_2)$ is given by

$$L_n(\alpha_1, \alpha_2) \triangleq \sum_j \begin{bmatrix} (h_j - h_{j-1}) I_3 \\ \frac{1}{2}(h_j^2 - h_{j-1}^2) I_3 \end{bmatrix} T_1^{-1} c_0^j \Lambda_n^j(\alpha_1, \alpha_2) \tag{25}$$

where the free strain of the jth lamina in the nth actuated area Λ_n^j is given by

$$\Lambda_n^j(\alpha_1, \alpha_2) = \begin{Bmatrix} d_{31} \\ d_{32} \\ 0 \end{Bmatrix} \frac{V_n^j}{\bar{h}_j} S_{\alpha_1}^n(\alpha_1) S_{\alpha_2}^n(\alpha_2) \tag{26}$$

and $\bar{h}_j$ is the thickness of the jth lamina defined by $\bar{h}_j \triangleq |h_j - h_{j-1}|$. The functions $S_{\alpha_1}^n(\alpha_1)$ and $S_{\alpha_2}^n(\alpha_2)$ describe the geometry of the nth actuated area in the shell. For areas that are generalized rectangles in the (α_1, α_2) plane, these functions are given by[5]

$$S_{\alpha_1}^n(\alpha_1) = H(\alpha_1 - \sigma_n^l) - H(\alpha_1 - \sigma_n^r) \tag{27}$$

$$S_{\alpha_2}^n(\alpha_2) = H(\alpha_2 - \lambda_n^l) - H(\alpha_2 - \lambda_n^r) \tag{28}$$

where H is the Heaviside step function and $(\sigma_n^l, \lambda_n^l), (\sigma_n^r, \lambda_n^r)$ are the locations of the left-lower and right-upper corners of the nth area in the (α_1, α_2) plane, respectively. For future use we also define the derivatives of $S_{\alpha_1}^n(\alpha_1)$ and $S_{\alpha_2}^n(\alpha_2)$ as

$$\Delta_{\alpha_1}^n(\alpha_1) = \delta(\alpha_1 - \sigma_n^l) - \delta(\alpha_1 - \sigma_n^r) \tag{29}$$

$$\Delta_{\alpha_2}^n(\alpha_1) = \delta(\alpha_2 - \lambda_n^l) - \delta(\alpha_2 - \lambda_n^r) \tag{30}$$

$$\Delta_{\alpha_1}'^n(\alpha_1) = \delta'(\alpha_1 - \sigma_n^l) - \delta'(\alpha_1 - \sigma_n^r) \tag{31}$$

$$\Delta_{\alpha_2}'^n(\alpha_1) = \delta'(\alpha_2 - \lambda_n^l) - \delta'(\alpha_2 - \lambda_n^r) \tag{32}$$

In the case of zero external load, the strains and curvatures developed in the shell when the active areas are driven by voltages sufficient to develop free strains of magnitude Λ_n are

$$\begin{Bmatrix} \epsilon_0 \\ \kappa \end{Bmatrix} = C_t^{-1} \sum_n^{N_a} L_n \tag{33}$$

The undamped equations of motion of a general piezolaminated anisotropic shell can now be stated in a compact form as

$$\bar{\rho}_t \ddot{\mathbf{x}} + \mathcal{K}\mathbf{x} = \frac{1}{A_1 A_2} \sum_n^{N_a} \mathcal{D} L_n(\alpha_1, \alpha_2, t) \tag{34}$$

where the (width normalized) total mass per unit area $\bar{\rho}_t$ is defined as

$$\bar{\rho}_t = \bar{\rho}_s + \bar{\rho}_a \triangleq \sum \rho_i \bar{h}_i + \sum_n^{N_a} \left[\sum_j \rho_j \bar{h}_j S_{\alpha_1}^n S_{\alpha_2}^n \right] \tag{35}$$

and the differential stiffness operator $\mathcal{K}$ is given by

$$\mathcal{K} \triangleq (1/A_1 A_2) \mathcal{D}^{\mathrm{T}} (1/A_1 A_2) C_t \mathcal{E} \tag{36}$$

$\mathcal{D}$ is a linear differential operator presented in full in a previous study.[11] These equations of motion can be reduced to the well-known cases of beams and plates and are fully compatible with similar results published in the literature.[11]

Two Common Cases of Laminae Arrangement

Most adaptive structures currently reported in the literature involve one structural lamina, with PZT actuators bonded to one or both of its surfaces.[1–3] Therefore, it is of some practical value to present results yielded by the current methodology for these particular cases.

In the case of actuators bonded to both surfaces, the laminate is symmetric about its reference plane, and consequently, the generalized stiffness matrix is block-diagonal. This implies that no stiffness related coupling between the extensional and bending displacements exists. Assuming for the sake of simplicity both the structural and actuator materials to be isotropic, we get the following expression for the diagonal blocks of the generalized stiffness matrix:

$$A_s = \frac{E_a h_a}{1 - \nu_a^2} \begin{bmatrix} \psi_\nu & \psi_\nu \nu_s & 0 \\ \psi_\nu \nu_s & \psi_\nu & 0 \\ 0 & 0 & \dfrac{\psi}{2(1+\nu_s)} \end{bmatrix} \tag{37}$$

$$A_a = \frac{E_a h_a}{1 - \nu_a^2} \begin{bmatrix} 2 & 2\nu_a & 0 \\ 2\nu_a & 2 & 0 \\ 0 & 0 & \dfrac{1}{1+\nu_a} \end{bmatrix} \tag{38}$$

and

$$D_s = \frac{E_a h_a h_s^2}{12(1 - \nu_a^2)} \begin{bmatrix} \psi_\nu & \psi_\nu \nu_s & 0 \\ \psi_\nu \nu_s & \psi_\nu & 0 \\ 0 & 0 & \dfrac{\psi}{2(1+\nu_s)} \end{bmatrix} \tag{39}$$

$$D_a = \frac{E_a h_a h_s^2}{12(1 - \nu_a^2)} \begin{bmatrix} \tau & \tau\nu_a & 0 \\ \tau\nu_a & \tau & 0 \\ 0 & 0 & \dfrac{\tau}{2(1+\nu_a)} \end{bmatrix} \tag{40}$$

The nondimensional thickness and stiffness related coefficients are defined as

$$T \triangleq h_s / h_a, \qquad \psi \triangleq T(E_s / E_a) \tag{41}$$

$$\tau \triangleq 6 + \frac{8}{T^2} + \frac{12}{T}, \qquad \psi_\nu \triangleq \psi \frac{1 - \nu_a^2}{1 - \nu_s^2} \tag{42}$$

To clearly observe the bending and extensional loading modes it is advantageous to examine the particular case of zero skew angles. In this case the induced-strain load vector L_n becomes

$$L_n = \frac{E_a h_a}{1 - \nu_a^2} \begin{Bmatrix} \Lambda_{\alpha_1\alpha_1}^{n+} + \nu_a \Lambda_{\alpha_2\alpha_2}^{n+} \\ \nu_a \Lambda_{\alpha_1\alpha_1}^{n+} + \Lambda_{\alpha_2\alpha_2}^{n+} \\ 0 \\ \dfrac{h_s}{2}\left(\dfrac{1}{T} + 1\right)(\Lambda_{\alpha_1\alpha_1}^{n-} + \nu_a \Lambda_{\alpha_2\alpha_2}^{n-}) \\ \dfrac{h_s}{2}\left(\dfrac{1}{T} + 1\right)(\nu_a \Lambda_{\alpha_1\alpha_1}^{n-} + \Lambda_{\alpha_2\alpha_2}^{n-}) \\ 0 \end{Bmatrix} S_{\alpha_1}^n(\alpha_1) S_{\alpha_2}^n(\alpha_2) \tag{43}$$

where $\Lambda_{\alpha_i\alpha_i}^{n+}$ and $\Lambda_{\alpha_i\alpha_i}^{n-}$ denote the sum and difference, respectively, of the free strain in the α_i direction for the nth actuated area. For many piezoceramics $d_{31} = d_{32}$ (Ref. 6), yielding $\Lambda_{\alpha_1\alpha_1}^n = \Lambda_{\alpha_2\alpha_2}^n$ and resulting in the induced-strain load vector

$$L_n = \frac{E_a h_a}{1 - \nu_a} \begin{Bmatrix} \Lambda_n^+ \\ \Lambda_n^+ \\ 0 \\ \dfrac{h_s}{2}\left(\dfrac{1}{T} + 1\right)\Lambda_n^- \\ \dfrac{h_s}{2}\left(\dfrac{1}{T} + 1\right)\Lambda_n^- \\ 0 \end{Bmatrix} S_{\alpha_1}^n(\alpha_1) S_{\alpha_2}^n(\alpha_2) \tag{44}$$

This leads to the expression of the reference plane strains and curvatures as

$$\epsilon_0 = \sum_{n=1}^{N_a}\left[\Lambda_n^+ \Big/ \left(\psi\frac{1+\nu_s}{1+\nu_a}+2\right)\right]\begin{Bmatrix}1\\1\\0\end{Bmatrix} \tag{45}$$

$$\kappa = \sum_{n=1}^{N_a}\left[6\left(\frac{1}{T}+1\right)\left(\frac{1}{h_s}\right)\Big/\left(\psi_\nu\frac{1+\nu_s}{1+\nu_a}+\tau\right)\right]\Lambda_n^-\begin{Bmatrix}1\\1\\0\end{Bmatrix} \tag{46}$$

When $T \gg 1$ the curvatures can be approximated by

$$\kappa = \sum_{n=1}^{N_a}\left[6\left(\frac{1}{h_s}\right)\Big/\left(\psi_\nu\frac{1+\nu_s}{1+\nu_a}+6\right)\right]\Lambda_n^-\begin{Bmatrix}1\\1\\0\end{Bmatrix} \tag{47}$$

As can be clearly seen from the expressions for the induced strains and curvatures, the efficiency of the piezoelectric actuators is inversely proportional to the stiffness ratio ψ. Furthermore, it can be seen that by exciting the top and bottom actuators with the same voltage of opposite sign (phase shift of 180 deg), we get $\Lambda_n^+ = 0$ and $\Lambda_n^- = 2\Lambda_n$, so that only bending displacements are excited, and with greater efficiency. By using zero phase shift, only extensional displacements are excited.

In the case of a single actuator bonded to a single structural lamina, the laminate is not symmetric about the reference plane and the extensional and bending displacements are coupled. The coupling effect, however, is slight and can be neglected. Assuming an isotropic case and neglecting the coupling we get the following expressions for the blocks of the generalized stiffness matrix:

$$A_a = \frac{E_a h_a}{1-\nu_a^2}\begin{bmatrix}1 & \nu_a & 0\\ \nu_a & 1 & 0\\ 0 & 0 & \dfrac{1}{2(1+\nu_a)}\end{bmatrix} \tag{48}$$

Because this laminate is not symmetric with respect to the active laminae, the B_s matrix vanishes, whereas B_a assumes the form

$$B_a = \frac{E_a h_a h_s}{2(1-\nu_a^2)}\left(\frac{1}{T}+1\right)\begin{bmatrix}1 & \nu_a & 0\\ \nu_a & 1 & 0\\ 0 & 0 & \dfrac{1}{2(1+\nu_a)}\end{bmatrix} \tag{49}$$

The matrices A_s and D_s remain unchanged from the preceding case, whereas

$$D_a = \frac{E_a h_a h_s^2}{12(1-\nu_a^2)}\begin{bmatrix}\tau_l & \tau_l\nu_a & 0\\ \tau_l\nu_a & \tau_l & 0\\ 0 & 0 & \dfrac{\tau_l}{2(1+\nu_a)}\end{bmatrix} \tag{50}$$

where

$$\tau_l \triangleq 3 + (4/T) + (6/T^2) \tag{51}$$

In the case of zero skew angles, the induced-strain load vector in this case is

$$\boldsymbol{L}_n = \frac{E_a h_a \Lambda_n}{1-\nu_a}\begin{Bmatrix}1\\1\\0\\ \dfrac{h_s}{2}\left(\dfrac{1}{T}+1\right)\\ \dfrac{h_s}{2}\left(\dfrac{1}{T}+1\right)\\0\end{Bmatrix} S_{\alpha_1}^n(x)S_{\alpha_2}^n(y) \tag{52}$$

and the reference plane strains and curvatures are

$$\epsilon = \sum_{n=1}^{N_a}\left[\Lambda_n \Big/ \left(\psi\frac{1+\nu_s}{1+\nu_a}+1\right)\right]\begin{Bmatrix}1\\1\\0\end{Bmatrix} \tag{53}$$

$$\kappa = \sum_{n=1}^{N_a}\left[3\left(1+\frac{1}{T}\right)\left(\frac{1}{h_s}\right)\Lambda_n \Big/ \left(\psi_\nu\frac{1+\nu_s}{1+\nu_a}+\tau_l\right)\right]\begin{Bmatrix}1\\1\\0\end{Bmatrix} \tag{54}$$

Generalized Sensing

The voltage measured across the lth lamina in the mth sensory area due to mechanically induced displacement is given by

$$\tilde{V}_m^l = \frac{1}{C_m^l}\iint_{A_m}\frac{1}{A_1 A_2}[\epsilon_0 \quad \kappa]\begin{Bmatrix}\boldsymbol{e}_m^l\\ \tilde{h}_l\boldsymbol{e}_m^l\end{Bmatrix}\mathrm{d}A \tag{55}$$

where C_m^l is the capacitance of the aforementioned piezoelement, which is given by

$$C_m^l = \iint_{A_n}\frac{\varepsilon_m^l}{h^l}\,\mathrm{d}A \tag{56}$$

and $\tilde{h}_l \triangleq \frac{1}{2}(h_l - h_{l-1})$ is the location of the central plane of the lth lamina. A_m is the area of the mth sensory area, and $\mathrm{d}A = A_1 A_2\,\mathrm{d}\alpha_1\,\mathrm{d}\alpha_2$.

Equation (55) shows that the measured voltage is proportional to the integral of the strain of the sensory laminae over their central plane areas. Because strains and curvatures do not normally appear as elements of the state of discretized structures, they should be substituted in Eq. (55) by shell translations and rotations, as was shown by Pletner et al.[14]

Governing Equations for Static and Dynamic Response

The static response of a thin continuous shell in the absence of external loading can be stated as

$$\frac{1}{A_1 A_2}\mathcal{D}\begin{Bmatrix}\boldsymbol{N}\\ \boldsymbol{M}\end{Bmatrix} = 0 \tag{57}$$

where $\mathcal{D}$ is a linear differential operator given by

$$\mathcal{D} = [\mathcal{N}\ \mathcal{M}] \tag{58}$$

where

$$\mathcal{N} \triangleq \begin{bmatrix}-\dfrac{\partial}{\partial\alpha_1}\cdot A_2 & A_{2,\alpha_1} & -\left[\dfrac{\partial}{\partial\alpha_2}\cdot A_1 + A_{1,\alpha_2}\right]\\ A_{1,\alpha_2} & -\dfrac{\partial}{\partial\alpha_2}\cdot A_1 & -\left[\dfrac{\partial}{\partial\alpha_1}\cdot A_2 + A_{2,\alpha_1}\right]\\ \dfrac{A_1 A_2}{R_1} & \dfrac{A_1 A_2}{R_2} & 0\end{bmatrix} \tag{59}$$

and

$$\mathcal{M} \triangleq \begin{bmatrix}-\dfrac{1}{R_1}\dfrac{\partial}{\partial\alpha_1}\cdot A_2 & \dfrac{1}{R_1}A_{2,\alpha_1} & -\dfrac{1}{R_1}\left[\dfrac{\partial}{\partial\alpha_2}\cdot A_1 + A_{1,\alpha_2}\right]\\ \dfrac{1}{R_1}A_{1,\alpha_2} & -\dfrac{1}{R_1}\dfrac{\partial}{\partial\alpha_2}\cdot A_1 & -\dfrac{1}{R_1}\left[\dfrac{\partial}{\partial\alpha_1}\cdot A_2 + A_{2,\alpha_1}\right]\\ \mathcal{M}^1 & \mathcal{M}^2 & \mathcal{M}^3\end{bmatrix} \tag{60}$$

The operators $\mathcal{M}^i$, $i = 1, 2, 3$, are defined as

$$\mathcal{M}^1 \triangleq \left(\frac{A_{1,\alpha_2}}{A_2}\right)_{\alpha_2} - \frac{\partial}{\partial\alpha_1}\cdot\frac{1}{A_1}\frac{\partial}{\partial\alpha_1}\cdot A_2 \tag{61}$$

$$\mathcal{M}^2 \triangleq \left(\frac{A_{2,\alpha_1}}{A_1}\right)_{\alpha_1} - \frac{\partial}{\partial\alpha_2}\cdot\frac{1}{A_2}\frac{\partial}{\partial\alpha_2}\cdot A_1 \tag{62}$$

$$\mathcal{M}^{\Delta}= -\left\{\frac{\partial}{\partial\alpha_1}\cdot\frac{1}{A_1}\cdot\left[\frac{\partial}{\partial\alpha_2}\cdot A_1 + A_{1,\alpha_2}\right] + \frac{\partial}{\partial\alpha_2}\cdot A_2\cdot\left[\frac{\partial}{\partial\alpha_1}\cdot A_2 + A_{2,\alpha_1}\right]\right\} \tag{63}$$

Introducing Eq. (18) into Eq. (57) and moving the induced strain force and moment resultants to the right-hand side, we get the governing equations for the static response of a laminated shell with active laminae in terms of the free strain of these laminae:

$$\mathcal{K}\mathbf{x} = \frac{1}{A_1 A_2}\sum_{n}^{N_a}\mathcal{D}\mathbf{h}_n(\alpha_1, \alpha_2) \tag{64}$$

where the differential stiffness operator $\mathcal{K}$ is given by Eq. (36). The right-hand side of Eq. (64) calls for various differentiations of the Heaviside step function. These derivatives and their physical meaning in the context of induced-strain actuation are given by Wang and Rogers[5] and are further clarified in the sequel.

Whenever the stiffness of the active laminae is to be neglected, a stiffness operator $\mathcal{K}$ consisting solely of the contributions of the geometrically continuous laminae can be defined by substituting C_s for C_t in Eq. (36). By substituting $\mathcal{K}$ for $\mathcal{K}$ in Eq. (64), we neglect the stiffnesses of the active laminae and make this an approximate solution. This is justified for low active-to-passive laminae stiffness ratios. In other cases the geometrically nonhomogeneous operator $\mathcal{K}$ should be used, and Eq. (64) should be solved using numerical methods.

To obtain the undamped dynamic response we add the inertia term $\bar{\rho}_t\ddot{\mathbf{x}}$ to the governing Eq. (64). This leads to the equations of motion

$$\bar{\rho}_t\ddot{\mathbf{x}} + \mathcal{K}\mathbf{x} = \frac{1}{A_1 A_2}\sum_{n}^{N_a}\mathcal{D}\mathbf{h}_n(\alpha_1, \alpha_2, t) \tag{65}$$

where the (width normalized) total mass per unit area $\bar{\rho}_t$ is defined as

$$\bar{\rho}_t = \bar{\rho}_s + \bar{\rho}_a \stackrel{\Delta}{=} \sum\rho_i\bar{h}_i + \sum_{n}^{N_a}\left[\sum_{j}\rho_j\bar{h}_j S^n_{\alpha_1} S^n_{\alpha_2}\right] \tag{66}$$

Analogously to the static case, the mass of the active laminae may be neglected by substituting $\bar{\rho}_s$ and $\mathcal{K}$ in Eq. (34).

The traction or displacement type boundary conditions for Eqs. (34) and (35) are given in Table 2, where the superscript b refers to the value of the coordinate at boundary. The transverse shear force resultants are defined in Ref. 15 as

$$Q_4 = (1/A_1A_2)\left[(A_2M_1)_{,\alpha_1} + (A_1M_6)_{,\alpha_2} + M_6(A_1)_{,\alpha_2} - M_2(A_2)_{,\alpha_1}\right] \tag{67}$$

$$Q_5 = (1/A_1A_2)\left[(A_2M_6)_{,\alpha_1} + (A_1M_2)_{,\alpha_2} + M_6(A_2)_{,\alpha_1} - M_1(A_1)_{,\alpha_2}\right] \tag{68}$$

As shown by Soedel,[15] the twisting moment and shear boundary conditions are related, and so only four independent conditions may be specified on each boundary. These are sometimes called the Kirchhoff boundary conditions, and they appear in the right-hand side of Table 2, where the effective stress resultants are defined as

$$V_4 = Q_4 + (1/A_2)M_{6,\alpha_2} \tag{69}$$

Table 2 Boundary conditions for a general thin shell

Poisson form		Kirchhoff form	
$\alpha_1 = \alpha_1^b$	$\alpha_2 = \alpha_2^b$	$\alpha_1 = \alpha_1^b$	$\alpha_2 = \alpha_2^b$
N_1 or u	N_2 or v	N_1 or u	N_2 or v
N_6 or v	N_6 or u	T_6^2 or v	T_6^1 or u
Q_4 or w	Q_5 or w	V_4 or w	V_5 or w
M_1 or β_1	M_2 or β_2	M_1 or β_1	M_2 or β_2
M_6 or β_2	M_6 or β_1	—	—

$$V_5 = Q_5 + (1/A_1)M_{6,\alpha_2} \tag{70}$$

$$T_6^i = N_6 + (M_6/R_i) \tag{71}$$

where $i = 1, 2$.

To simulate real structures, damping has to be added to the equations of motion. Following Meirovitch,[16] we can define two possible models for the dissipative energy in the vibrating shell: the proportional damping model and the structural damping model. Proportional damping is assumed to be proportional to the mass operator through the constant α and the stiffness operator through the constant β, yielding the following expression for the dissipative energy operator:

$$\mathcal{C} = \alpha\bar{\rho}_t + \beta\mathcal{K} \tag{72}$$

and resulting in the damped equations of motion

$$\bar{\rho}_t\ddot{\mathbf{x}} + \mathcal{C}\dot{\mathbf{x}} + \mathcal{K}\mathbf{x} = \frac{1}{A_1 A_2}\sum_{n}^{N_a}\mathcal{D}\mathbf{h}_n(\alpha_1, \alpha_2, t) \tag{73}$$

In the case of steady-state purely harmonic excitation, the velocity term can be expressed as

$$\dot{\mathbf{x}} = j\omega\mathbf{x} \tag{74}$$

where $j = \sqrt{(-1)}$. By choosing $\alpha = 0$ and $\beta = \gamma/\omega$, we get

$$\bar{\rho}_t\ddot{\mathbf{x}} + (1 + j\gamma)\mathcal{K}\mathbf{x} = \frac{1}{A_1 A_2}\sum_{n}^{N_a}\mathcal{D}\mathbf{h}_n(\alpha_1, \alpha_2, t) \tag{75}$$

where γ is referred to as the structural damping factor. Analytical solutions of the equations of motion are possible when $\bar{\rho}_t$ and $\mathcal{K}$ are homogeneous throughout the spatial domain of the structure (mass and stiffness of the piezoelectric elements is neglected), and the specified boundary conditions allow closed-form solutions. In other cases, these equations have to be integrated numerically.

Structures with a Single Passive Lamina Between Two Active Laminae

Isotropic Plates

For a plate defined in the Cartesian coordinate system x, y, z so that $\alpha_1 \equiv x$, $\alpha_2 \equiv y$, $\alpha_3 \equiv z$, the operator $\mathcal{E}$ becomes

$$\mathcal{E} = \begin{bmatrix} \frac{\partial}{\partial x} & 0 & 0 \\ 0 & \frac{\partial}{\partial y} & 0 \\ \frac{\partial}{\partial y} & \frac{\partial}{\partial x} & 0 \\ 0 & 0 & -\frac{\partial^2}{\partial x^2} \\ 0 & 0 & -\frac{\partial^2}{\partial y^2} \\ 0 & 0 & -2\frac{\partial^2}{\partial x\partial y} \end{bmatrix} \tag{76}$$

This yields the following curvature vector:

$$\boldsymbol{\kappa} = -\begin{Bmatrix} w_{,xx} \\ w_{,yy} \\ 2w_{,xy} \end{Bmatrix} \tag{77}$$

which is, of course, a well-known result. The differential operator $\mathcal{D}$ becomes

$$\mathcal{D} = -\begin{bmatrix} \frac{\partial}{\partial x} & 0 & \frac{\partial}{\partial y} & 0 & 0 & 0 \\ 0 & \frac{\partial}{\partial y} & \frac{\partial}{\partial x} & 0 & 0 & 0 \\ 0 & 0 & 0 & \frac{\partial^2}{\partial x^2} & \frac{\partial^2}{\partial y^2} & 2\frac{\partial^2}{\partial x\partial y} \end{bmatrix} \tag{78}$$

and the total stiffness operator $\mathcal{K}$ assumes the form

$$\mathcal{K} = \mathcal{D}^T \mathcal{E} = \left[\begin{array}{c|c|c} \mathcal{K}_1 & \mathcal{K}_1 & 0 \\ \hline \mathcal{K}_1 & \mathcal{K}_2 & 0 \\ \hline 0 & 0 & -\mathcal{K}_3 \end{array}\right] \tag{79}$$

where the bending stiffness operator $\mathcal{K}_3$ is

$$\mathcal{K}_3 = \frac{E_a h_a h_s^2}{12(1-\nu_a^2)} \left\{ \psi_\nu \left(\frac{\partial^4}{\partial x^4} + \frac{\partial^4}{\partial y^4} \right) + 2\left(\psi_\nu \nu_s + \frac{1}{1+\nu_s} \right) \times \frac{\partial^4}{\partial x^2 \partial y^2} + \tau \left[\sum_n^{N_a} \Delta_x^n(x) S_y^n(y) \frac{\partial^4}{\partial x^4} + \sum_n^{N_a} \Delta_y^n(y) S_x^n(x) \frac{\partial^4}{\partial y^4} + \nu_a \sum_n^{N_a} \left(\Delta_x^n(x) S_y^n(y) + \Delta_y^n(y) S_x^n(x) + \frac{2}{1+\nu_a} \Delta_x^n(x) \Delta_y^n(y) S_x^n(x) S_y^n(y) \right) \frac{\partial^4}{\partial x^2 \partial y^2} \right] \right\} \tag{80}$$

and the extensional stiffness operators are presented in a previous study.[11]

The transverse static and dynamic responses can now be stated as

$$\mathcal{K}_3 w = \frac{E_a h_a h_s [1 + (1/T)]}{1-\nu_a} \sum_n^{N_a} \Lambda_n^- \left[\Delta_x^n(x) S_y^n(y) + \Delta_y^n(y) S_x^n(x) \right] \tag{81}$$

$$\bar{\rho}_1 \ddot{w} + \mathcal{K}_3 w = \frac{E_a h_a h_s [1 + (1/T)]}{1-\nu_a} \times \sum_n^{N_a} \Lambda_n^-(t) \left[\Delta_x^n(x) S_y^n(y) + \Delta_y^n(y) S_x^n(x) \right] \tag{82}$$

Orthotropic Plates

This section extends the earlier results for orthotropic structural laminae in the context of plates equipped with symmetrically bonded actuator pairs. Assuming that the material symmetry axes coincide with the coordinate system, the stiffness matrix for the passive laminae becomes

$$c^{(2)} = \begin{bmatrix} c_{11} & c_{12} & 0 \\ c_{21} & c_{22} & 0 \\ 0 & 0 & c_{66} \end{bmatrix} \tag{83}$$

The stiffness matrices for the active laminae remain unchanged. The blocks $A_{s,a}$ and $D_{s,a}$ of the generalized stiffness matrix assume the form

$$A_s = \frac{E_a h_a}{1-\nu_a^2} \begin{bmatrix} \eta_{11} & \eta_{12} & 0 \\ \eta_{21} & \eta_{22} & 0 \\ 0 & 0 & \eta_{66} \end{bmatrix} \tag{84}$$

$$A_a = \frac{E_a h_a}{1-\nu_a^2} \begin{bmatrix} 2 & 2\nu_a & 0 \\ 2\nu_a & 2 & 0 \\ 0 & 0 & \dfrac{1}{1+\nu_a} \end{bmatrix} \tag{85}$$

$$B_s = \frac{E_a h_a h_s^2}{12(1-\nu_a^2)} \begin{bmatrix} \eta_{11} & \eta_{12} & 0 \\ \eta_{21} & \eta_{22} & 0 \\ 0 & 0 & \eta_{66} \end{bmatrix} \tag{86}$$

$$B_a = \frac{E_a h_a h_s^2}{12(1-\nu_a^2)} \begin{bmatrix} \tau & \tau\nu_a & 0 \\ \tau\nu_a & \tau & 0 \\ 0 & 0 & \dfrac{\tau}{2(1+\nu_a)} \end{bmatrix} \tag{87}$$

where the nondimensional stiffness coefficients η_{ij} are defined as

$$\eta_{ij} \triangleq \frac{T(1-\nu_a^2)}{E_a} c_{ij} \tag{88}$$

The reference plane strains are

$$\epsilon_0 = (1+\nu_a)\, \xi_\epsilon \sum_n^{N_a} \Lambda_n^+ \begin{Bmatrix} 1 \\ 1 \\ 0 \end{Bmatrix} \tag{89}$$

and the curvatures

$$\kappa = 6(1+\nu_a) \left(\frac{1}{T} + 1 \right) \left(\frac{1}{h_s} \right) \xi_\kappa \sum_n^{N_a} \Lambda_n^- \begin{Bmatrix} 1 \\ 1 \\ 0 \end{Bmatrix} \tag{90}$$

where the nondimensional parameters ξ_ϵ and ξ_κ are defined by

$$\xi_\epsilon \triangleq \frac{2(1-\nu_a) + \eta_{11} - \eta_{12}}{(2+\eta_{11})(2+\eta_{22}) - (2\nu_a + \eta_{12})^2} \tag{91}$$

$$\xi_\kappa \triangleq \frac{\tau(1-\nu_a) + \eta_{11} - \eta_{12}}{(\tau+\eta_{11})(\tau+\eta_{22}) - (\tau\nu_a + \eta_{12})^2} \tag{92}$$

The components of the operator matrix $\mathcal{K}$ can be obtained for the orthotropic case by formally substituting η_{11} for ψ_ν, η_{12} for $\psi_\nu \nu_s$, and $2\eta_{66}$ for $1/(1+\nu_s)$ in the isotropic expressions [Eqs. (79) and (80)]. Substituting these components into the expressions for the static and dynamic responses of the isotropic plate [Eq. (82)] yields the responses of the orthotropic case.

For bending motion in rectangular plates in which the transverse displacement function can be expressed as a product of two single-coordinate functions, $w(\alpha_1 \alpha_2) = w_1(\alpha_1) w_2(\alpha_2)$, Eq. (55) becomes

$$\tilde{V}_m^l = -\frac{h e_{31}^{l,m}}{C_{l,m}} \int_{\alpha_m^l}^{\sigma_m^r} w_1'(\alpha_1)\, d\alpha_1 - \frac{h e_{32}^{l,m}}{C_{l,m}} \int_{\lambda_m^l}^{\lambda_m^r} w_2'(\alpha_2)\, d\alpha_2 = -\eta_{l,m}^1 \left[w_1(\alpha_1^{l,R}) - w_1(\alpha_1^{l,L}) \right] - \eta_{l,m}^2 \left[w_2(\alpha_2^{l,B}) - w_2(\alpha_2^{l,T}) \right] \tag{93}$$

The slope differences in Eq. (93) can be easily incorporated into various structural discretization schemes.

Cylindrical Shells

For a circular cylindrical shell of radius a ($A_2 = R_2 = a$) the preferred coordinate system is cylindrical, such that $\alpha_1 \equiv \theta$, $\alpha_2 \equiv z$, and $\alpha_3 \equiv r$. The differential operators $\mathcal{E}$ and $\mathcal{D}$ for this case are given by

$$\mathcal{E} = \begin{bmatrix} a\dfrac{\partial}{\partial\theta} & 0 & 0 \\ 0 & \dfrac{\partial}{\partial z} & 0 \\ \dfrac{\partial}{\partial z} & a\dfrac{\partial}{\partial\theta} & 0 \\ 0 & 0 & -a\dfrac{\partial^2}{\partial\theta^2} \\ 0 & \dfrac{1}{a}\dfrac{\partial}{\partial z} & -\dfrac{1}{a}\dfrac{\partial^2}{\partial z^2} \\ 0 & \dfrac{\partial}{\partial\theta} & -2\dfrac{\partial^2}{\partial\theta\partial z} \end{bmatrix} \tag{94}$$

$$\mathcal{D}^T = \begin{bmatrix} a\dfrac{\partial}{\partial\theta} & 0 & \dfrac{\partial}{\partial z} & 0 & 0 & 0 \\ 0 & \dfrac{\partial}{\partial z} & a\dfrac{\partial}{\partial\theta} & 0 & 0 & 0 \\ 0 & 1 & 0 & a\dfrac{\partial^2}{\partial\theta^2} & \dfrac{1}{a}\dfrac{\partial^2}{\partial z^2} & (1+a)\dfrac{\partial^2}{\partial\theta\partial z} \end{bmatrix} \tag{95}$$

The stiffness operator $\mathcal{K}$ for a cylindrical shell becomes

$$\mathcal{K} = \frac{1}{a^2}\mathcal{D}^t\mathcal{E} = -\frac{1}{a^2}\begin{bmatrix} \mathcal{K}_1 & \mathcal{K}_2 & 0 \\ \mathcal{K}_4 & \mathcal{K}_5 & 0 \\ \mathcal{K}_7 & \mathcal{K}_8 & -\mathcal{K}_9 \end{bmatrix} \tag{96}$$

where the bending and coupled extensional-bending operators $\mathcal{K}_i$, $i = 1, 2, 3$, are

$$\mathcal{K}_1 = \frac{E_a h_a h_s^2}{12(1-\nu_a^2)} a\left(\psi_\nu \nu_s + 2\nu_a \sum_n^{N_a} S_\theta^n(\theta) S_z^n(z)\right)\frac{\partial}{\partial\theta} \tag{97}$$

$$\mathcal{K}_2 = \frac{E_a h_a h_s^2}{12(1-\nu_a^2)}\left[a^2\left(\psi_\nu + 2\nu_a \sum_n^{N_a} S_\theta^n(\theta) S_z^n(z)\right)\frac{\partial}{\partial z} + \left(\psi_\nu + \tau\sum_n^{N_a}\Delta_z^n(z) S_\theta^n(\theta)\right)\frac{\partial^3}{\partial z^3} + a^2(a+1) \times\left(\frac{\psi}{2(1+\nu_s)} + \frac{\tau}{2(1+\nu_a)}\sum_n^{N_a}\Delta_\theta^n(\theta) S_z^n(z)\right)\frac{\partial^3}{\partial\theta^2\partial z}\right] \tag{98}$$

$$\mathcal{K}_3 = \frac{E_a h_a h_s^2}{12(1-\nu_a^2)}\left[a^4\left(\psi_\nu + 2\nu_a \sum_n^{N_a}\Delta_\theta^n(\theta) S_z^n(z)\right)\frac{\partial^4}{\partial\theta^4} + \left(\psi_\nu + 2\nu_a\sum_n^{N_a}\Delta_z^n(z) S_\theta^n(\theta)\right)\frac{\partial^4}{\partial z^4} + a^2(a+1) \times\left(\frac{\psi}{2(1+\nu_s)} + \frac{\tau}{2(1+\nu_a)}\sum_n^{N_a}\Delta_\theta^n(\theta)\Delta_z^n(z)\right)\frac{\partial^3}{\partial\theta^2\partial z}\right] \tag{99}$$

and the purely extensional operators are presented in a previous study.[11] It is clear that in this case the transverse displacement is coupled to the in-plane displacements. This coupling is geometric in origin and is a general result for all cylindrical shells.

For orthotropic cylindrical panels in which the material and structural axes coincide, the stiffness operator components can be obtained directly from Eqs. (99) by formally substituting η_{11} for ψ_ν, η_{12} for $\psi_\nu\nu_s$, and η_{66} for $[\psi/2(1+\nu_s)]$.

Sensing equations are equivalent to the flat plate case and can be restated in cylindrical coordinates as

$$\tilde{V}_m^l = \frac{1}{C_m^l}\int_{\sigma_m^l}^{\sigma_m^r}\int_{\lambda_m^l}^{\lambda_m^r}\tilde{h}_l e_{31}^{lm}\left[\epsilon_{\theta\theta}^0 + \epsilon_{zz}^0 + \tilde{h}_l(\kappa_{\theta\theta} + \kappa_{zz})\right]\mathrm{d}\theta\,\mathrm{d}z \tag{100}$$

Numerical Investigation

Here the results of the preceding section are validated using the ANSYS® coupled-field piezoelectric three-dimensional solid element.[17] The maximum static transverse displacement of the structure is found using the following models: three-dimensional model with actuators modeled by coupled-field elements under electrical loading, denoted coupled solid model; three-dimensional model with actuator modeled by structural elements under equivalent mechanical loading, denoted pin-force solid model; and beam or shell element model neglecting actuator stiffness under mechanical loading, denoted beam/plate model. All models were meshed so that their maximum displacements for on-resonance excitation at steady state coincided within $\pm 1\%$.

The force couples and moments applied by the piezoelectric elements on the structure were found using the results of the current theory. These force couples (in case of three-dimensional models) and moments (in case of beam and shell models) were applied at the edges of the actuators, and the resulting displacements were compared with those resulting from the application of voltage to the piezoelectric elements. To model various material properties and stiffness ratios between the laminae three materials were used: steel, aluminum, and graphite/epoxy.

Table 3 Maximum transverse displacement for a simply supported plate (in micrometers per volt)

	Steel	Aluminum	Graphite/epoxy
Coupled solid model (1)	0.121	0.297	0.515
Pin-force solid model (2)	0.125	0.310	0.544
Plate model (3)	0.117	0.265	——
Error (1)–(2), %	3.20	4.19	5.33
Error (1)–(3), %	3.31	10.77	——

Table 4 Maximum transverse displacement for a cylindrical panel (in micrometers per volt)

	Steel	Aluminum	Graphite/epoxy
Coupled solid model (1)	2.05	0.903	0.801
Pin-force solid model (2)	2.03	0.918	0.805
Plate model (3)	2.19	0.765	——
Error (1)–(2), %	3.20	4.19	5.33
Error (1)–(3), %	3.31	10.77	——

Plate with One Actuator Pair

For this analysis we used an all-round simply supported plate of dimensions $380 \times 300 \times 1.96$ mm. Two actuators of dimension $60 \times 40 \times 0.1905$ mm were assumed to be perfectly bonded to the upper and lower surfaces of the plate, at its center. For the solid model the plate was meshed into 2 elements in the thickness direction and into 30×15 elements in the in-plane directions. The element type was solid45. The actuators were each meshed into 1 element in the thickness direction and 10×5 elements in the in-plane directions, using the solid5 piezoelectric elements. For the shell model the plate was meshed into 10×10 shell63 elastic shell elements. The results for the plate are given in Table 3.

Cylindrical Panel with One Actuator Pair

The cylindrical panel chosen for this case was 60 cm long, 0.2 mm thick, with a nominal radius of 38.2 cm, and spanning 60 deg. The panel was clamped at one of the short ends and actuated by two $50 \times 50 \times 0.1905$ mm PZT patches bonded to its upper and lower surfaces. This panel was modeled by a solid three-dimensional model and a shell-element two-dimensional model. In the solid model, the shell was meshed into 1 element in the thickness r direction and into 25×25 solid45 elements in the z and θ directions. The piezoelectric patches were modeled, as in preceding cases, with the solid5 coupled-field piezoelectric elements. The two-dimensional model meshed the shell's surface into 25×25 shell63 elements.

The results for the various loadings and models are presented in Table 4. There is excellent agreement between the electrically and mechanically loaded three-dimensional solid models. This agreement extends beyond the maximum deflections and is present also in the entire vibrational shape of the panel (see Fig. 3).

The two-dimensional shell element model, however, is much less accurate. This stems mainly from neglecting the stiffness contribution of the PZT actuator pair, which in this case is not very small with respect to the bending stiffness of the (thin) structural lamina.

Experimental Investigation

The experimental investigation was performed using a thin cantilever steel plate actuated by a single actuator pair, as shown in Fig. 4. This configuration was chosen because clamped boundary conditions are much easier to create than the idealized simply supported case. A single actuator pair at the root was used, ensuring its location at the area of maximum strain.

The purpose of the experiment was to validate the coupled-field finite element (FE) modeling technique, as well as the extended pin-force model presented earlier. This was done by determining the first fundamental frequency of the plate, exciting it on-resonance using the piezoelectric actuators, and obtaining the steady-state response. As a measure of this response, the strain at the root of the plate was measured using a strain gauge couple at the clamp (see Fig. 4). This strain was then compared to the strains found by the coupled-field FE model of the plate using the ANSYS harmonic analysis capability. This was done both for electrical loads and for the equivalent

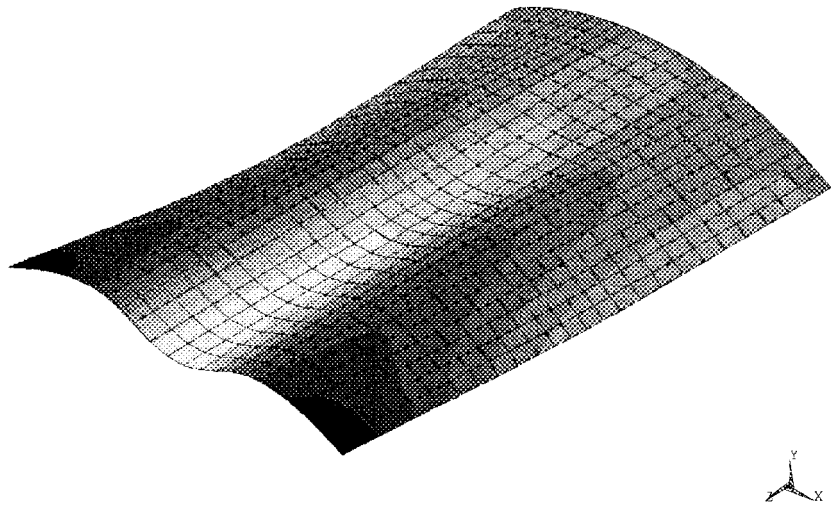

a) Under electrical loading

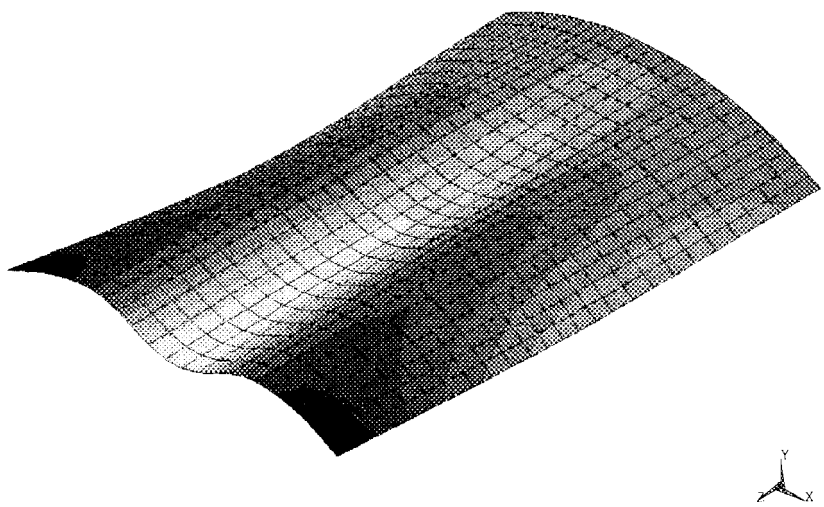

b) Under equivalent mechanical loading

Fig. 3 Deflection of cylindrical panel modeled with solid elements.

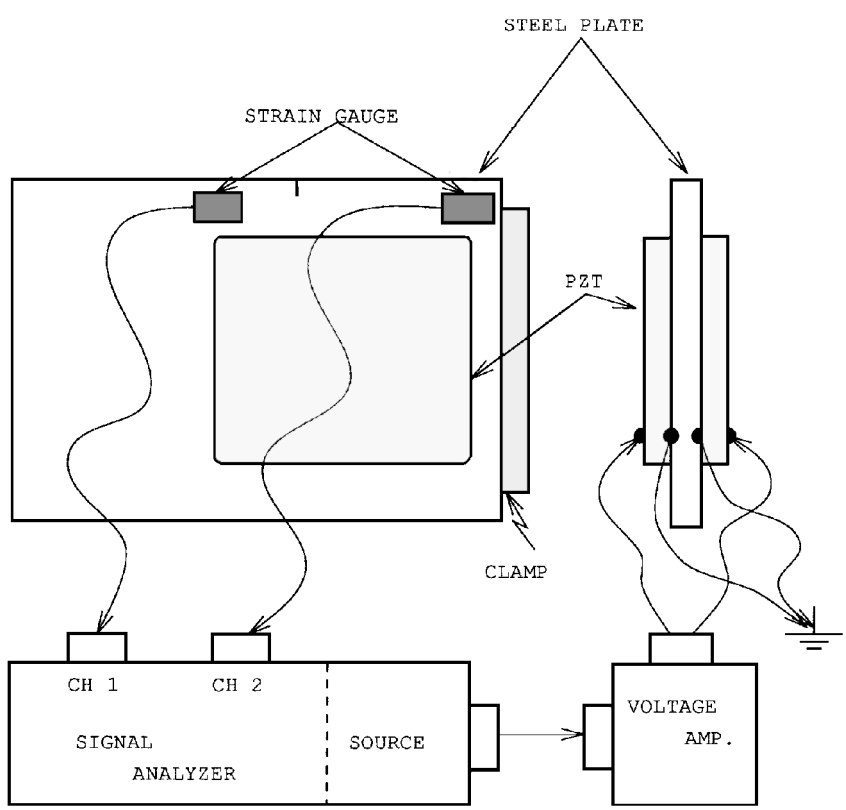

Fig. 4 Experimental setup.

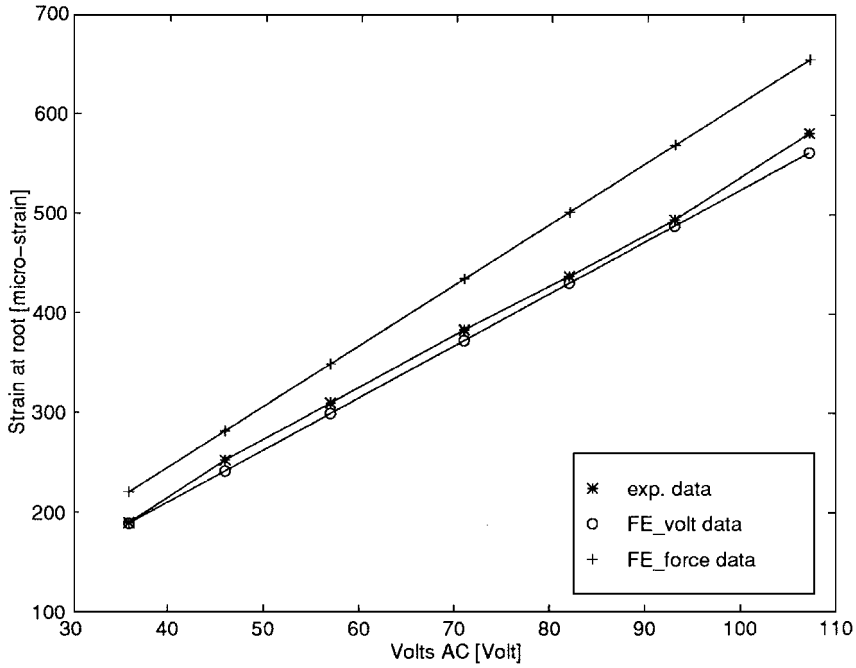

Fig. 5 Strain at root of plate at 40 Hz.

mechanical loads found using the pin-force model. The process was repeated for several amplitudes of excitation, and the results are shown in Fig. 5. To ensure the highest possible numerical accuracy, the damping coefficient scaling the stiffness matrix in the FE model was set so that the response found using the FE model to the lowest driving voltage coincided with the experimental value to within $\pm 0.1\%$.

Discussion and Conclusions

Analytical Derivations

A general methodology for obtaining the static and dynamic response of anisotropic piezolaminated shells and the modeling of induced-strain piezoelectric actuation with equivalent mechanical loads was developed. This methodology was shown to be reducible to the particular cases of one structural lamina with one or two actuating laminae. Useful expressions were obtained for the determination of equivalent mechanical loads and piezoelectrically induced strains and curvatures. General equations for piezoelectric sensing were obtained, and several methods were proposed for calibrating piezoelectric sensors for the estimation of transverse displacements.

The general theory developed in this study was applied to the particular case of a single structural laminae sandwiched between piezoceramic actuators. This configuration was investigated numerically using the ANSYS FE program for an all-round simply supported plate with one actuator pair and a cantilever cylindrical panel with one actuator pair. An experimental investigation was performed on a cantilever steel plate with one actuator pair.

The numerical and experimental investigations validated the use of the modeling techniques developed in this research for static as well as dynamic excitations. In addition, the coupled-field capability of the ANSYS program was thoroughly investigated and validated experimentally.

FE Modeling of Piezoactuated Structures

For some time now, finite elements analysis (FEA) has been the method of choice for the analysis of structures that do not yield to closed-form solutions. In the context of smart structures, however, its role must be reassessed. The applicability of FEA to the smart structure design process should be investigated with respect to its capability of modeling the piezoelectric effects, and through them, the piezoelectric actuation and sensing. In addition, the method's possible use as a structural discretization scheme for controller design should be addressed. The piezoelectric modeling capability was investigated and shown to be in excellent agreement with both analytical and experimental results.

Although it is possible to model the actuators and sensors in smart structures with coupled-field elements, it is numerically expensive. This is due to the lack of coupled-field capability in many popular elements, such as beam and shell elements. In ANSYS, only two- and three-dimensional solids have coupled-field capability. Additionally, the electric degrees of freedom at the nodes of the coupled-field elements can significantly increase the dimension of the model. To avoid this numerical expense it is, therefore, advisable to replace the coupled-field elements by the appropriate structural elements and the equivalent mechanical loads found using the theory developed in this study. In some cases further reduction in model size can be obtained by neglecting the mass and stiffness contributions of the active and sensory laminae and by modeling the structure with one- and two-dimensional elements. This should only be done, however, for large structural-to-active stiffness and mass ratios.

Experimental Results and Conclusions

The experiment clearly demonstrated the feasibility of actuating flexible continuous structures with piezoceramic patches. Bending of a steel cantilever plate was achieved using both one and two active laminae. The excellent agreement between experimental results and those predicted by the coupled-field FE model suggests that the effects of the bonding lamina could justifiably be neglected for the system under investigation. The use of a piezoceramic patch in lieu of a strain gauge was shown to be very advantageous because the piezoceramic produces a clear, noise-free signal of the order of magnitude of 10 V and more and does not require any outside power source. In contrast, strain gauges require amplification, which introduces noise into the measurement and produce signals of the order of magnitude of millivolts. The piezoceramic patches were shown to perform well both as sensors and as actuators over a wide range of driving frequencies and amplitudes. This validated the modeling of electrical loads by the equivalent mechanical loads for the dynamic case. In the future, larger scale experiments, such as aircraft cabins, need to be performed in order to fully access the validity of piezoelectric actuation and sensing in closed-loop vibration and acoustic control applications.

References

[1]Crawley, F., and de Luis, J., "Use of Piezoelectric Actuators as Elements of Intelligent Structures," *AIAA Journal*, Vol. 25, No. 10, 1987, pp. 1373–1385.

[2]Chaudhry, Z., and Rogers, C., "The Pin-Force Model Revisited," *Journal of Intelligent Materials Systems and Structures*, Vol. 5, May 1994, pp. 347–354.

[3]Strambi, G., Barboni, R., and Gaudenzi, P., "Pin-Force and Euler-Bernoulli Models for Analysis of Intelligent Structures," *AIAA Journal*, Vol. 33, No. 9, 1995, pp. 1746–1749.

[4]Dimitriadis, E., Fuller, C., and Rogers, C., "Piezoelectric Actuators for Distributed Vibration Excitation of Thin Plates," *Journal of Vibrations and Acoustics*, Vol. 131, Jan. 1991, pp. 100–107.

[5]Wang, B., and Rogers, C., "Laminate Plate Theory for Spatially Distributed Induced Strain Actuators," *Journal of Composite Materials*, Vol. 25, April 1991, pp. 433–453.

[6]Clark, R., Flemming, M., and Fuller, C., "Piezoelectric Actuators for Distributed Vibrations Excitation of Thin Plates: A Comparison Between Theory and Experiment," *Journal of Vibrations and Acoustics*, Vol. 115, July 1993, pp. 332–339.

[7]Tzou, H., *Piezoelectric Shells*, Kluwer Academic, Norwell, MA, 1993.

[8]Miller, S., Oshman, Y., and Abramovich, H., "Model Control of Piezolaminated Anisotropic Rectangular Plates: Part 1 Modal Transducer Theory," *AIAA Journal*, Vol. 34, No. 9, 1996, pp. 1868–1875.

[9]Miller, S., Oshman, Y., and Abramovich, H., "Modal Control of Piezolaminated Anisotropic Rectangular Plates: Part 2 Control Theory," *AIAA Journal*, Vol. 34, No. 9, 1996, pp. 1876–1884.

[10]Pletner, B., and Abramovich, H., "Piezoelectric Sensors for Adaptive Suspensions of Vehicles," *Journal of Intelligent Materials Systems and Structures*, Vol. 34, Nov. 1995, pp. 34–56.

[11]Pletner, B., and Abramovich, H., "Actuation and Sensing in Piezolaminated Anisotropic Shells: Theoretical Numerical and Experimental Investigation," Faculty of Aerospace Engineering, TR TAE779, Technion—Israel Inst. of Technology, Haifa, Israel, June 1996.

[12]Park, C., Waltz, C., and Chopra, I., "Bending and Torsion Models of Beams with Induced-Strain Actuators," *Smart Materials and Structures*, Vol. 5, Feb. 1996, pp. 98–113.

[13]Sonti, V., and Jones, J., "Curved Piezoactuator Model for Active Vibration Control of Cylindrical Shells," *AIAA Journal*, Vol. 34, No. 5, 1996, pp. 1034–1040.

[14]Pletner, B., Idan, M., Abramovich, H., and Weller, T., "Balanced Acoustic Control of Flexible Structures," TR TAE784, Technion—Israel Inst. of Technology, Haifa, Israel, Sept. 1996.

[15]Soedel, W., *Vibrations of Shells and Plates*, Dekker, New York, 1981.

[16]Meirovitch, L., *Dynamics and Control of Structures*, Wiley, New York, 1990.

[17]ANSYS, "Ansys User's Manual–Revision 5.0," Swanson Analysis Systems, Canonsburg, PA, 1992.

A. M. Waas
Associate Editor